Applied Catalysis B: Environmental 233 (2018) 19–25

Contents lists available at ScienceDirect

Applied Catalysis B: Environmental

journal homepage: www.elsevier.com/locate/apcatb

Direct evidence of IR-driven hot electron transfer in metal-free plasmonic $W_{18}O_{49}$/Carbon heterostructures for enhanced catalytic H_2 production

Na Lu, Zhenyi Zhang*, Yue Wang, Benkang Liu, Lijiao Guo, Li Wang, Jindou Huang, Kuichao Liu, Bin Dong*

Key Laboratory of New Energy and Rare Earth Resource Utilization of State Ethnic Affairs Commission, Key Laboratory of Photosensitive Materials & Devices of Liaoning Province, School of Physics and Materials Engineering, Dalian Nationalities University, 18 Liaohe West Road, Dalian 116600, PR China

ARTICLE INFO

Keywords:
H_2 production
Photocatalysis
Electrospinning
Plasmonic semiconductor
Carbon fiber

ABSTRACT

Plasmonic nanostructures have received significant attention in the field of solar-to-fuels conversion, because they can collect and utilize abundant low-energy photons to generate high-energy hot electrons for producing green chemical fuels. However, the ultrafast relaxation process of hot electron often leads to poor quantum yields of plasmonic nanostructures. Herein, we construct the one-dimensional $W_{18}O_{49}$/Carbon heterostructure for employing low-cost electrospun carbon fibers as the "electron mediator" to hinder the relaxation of hot electron in plasmonic $W_{18}O_{49}$ nanowires. We confirm that the IR-excited plasmonic hot electrons in $W_{18}O_{49}$ nanowires can quickly transfer to carbon fibers within only ~50 fs in the $W_{18}O_{49}$/C heterostructure. This kinetics time is much shorter than the relaxation time of these hot electrons from high-energy surface plasmon (SP) to the ground state in $W_{18}O_{49}$ nanowires (~5.5 ps). As a result, upon low-energy IR-light excitation, the $W_{18}O_{49}$/C heterostructures exhibit nearly 2-fold enhancement on the catalytic H_2 production from ammonia borane as compared to single $W_{18}O_{49}$ nanowires. Wavelength-dependent catalytic tests further indicate that this plasmon-enhanced catalytic activity is induced by the ultrafast transport process of plasmonic hot electron due to the localized surface plasmon resonance.

1. Introduction

Effectively harvesting low-energy photons with low-cost photocatalysts for the production of H_2 from hydrogen-carrier molecules is a fascinating tactic to address the ever-growing demand on the clean and renewable energy [1–5]. In theory, the semiconductor with a narrow bandgap can realize the absorption of abundant infrared radiation (IR, 0.4–1.6 eV) that occupies more than half of solar spectrum (54.3%) [6–8]. However, this kind of semiconductor inevitably suffers fast recombination of photoinduced charge-carrier and poor redox ability, leading to low photocatalytic efficiency [9–12]. Alternatively, plasmonic nanostructures, such as noble metals and heavily doped semiconductors, with unique localized surface plasmon resonance (LSPR) offer a new promising opportunity to effectively collect and utilize abundant IR light for the H_2 production [13–17]. Unlike traditional semiconductor-based photocatalysts, plasmonic photocatalysts possess the tunable light absorption, ranging from visible to IR, and the big "energy window" to generate high-energy "hot electron" for the reduction of hydrogen-carrier molecules [18–24]. Especially, plasmonic semiconductor-based photocatalysts, such as WO_{3-x}, MoO_{3-x}, and $Cu_{2-x}S$, are the most attractive candidates for harvesting low-energy photons due to their broad and intense LSPR in IR region [25–28]. Recently, some groups have employed low-cost $W_{18}O_{49}$ nanowires as the plasmonic catalysts to boost the H_2 production from ammonia borane (NH_3BH_3) based on the IR-driven injection of plasmonic hot electrons [29,30]. Nevertheless, ultrafast relaxation process of these hot electrons often leads to recombination of photoinduced charge-carriers against the transport of hot electrons, resulting in the limited catalytic efficiency of $W_{18}O_{49}$ nanowires.

As an important metal-free conductive support, one-dimensional (1D) carbon fiber has attracted extensive attention because of its economical price, easy processibility, strong mechanical strength, and good chemical and thermal stability [31–33]. Moreover, the surfaces of carbon fibers contain a plenty of functional groups, such as hydroxyl, carboxyl, carbonyl, and so forth, which provide abundant active sites to allow the direct growth of inorganic nanocrystals on carbon fibers without requiring any "organic molecule linker" [34–36]. To date, 1D carbon fiber with the conductivity of 0.003–0.007 Ω cm has been widely used as the electron transport pathway for boosting separation or transfer of the charge-carriers in noble metal or semiconductor-based

* Corresponding authors.
E-mail addresses: zhangzy@dlnu.edu.cn (Z. Zhang), dong@dlnu.edu.cn (B. Dong).

https://doi.org/10.1016/j.apcatb.2018.03.073
Received 9 January 2018; Received in revised form 12 March 2018; Accepted 21 March 2018
Available online 22 March 2018

heterostructures [37–39]. However, the kinetics process of plasmon-induced hot electron in the plasmonic semiconductor/carbon fibers system has not been reported up until now. A deep understanding of this ultrafast process will motivate the development of low-cost non-metallic plasmonic photocatalyst for achieving highly-efficient IR-driven H_2 production.

In this work, we gave a successful attempt to construct 1D $W_{18}O_{49}$/C heterostructure through direct growth of plasmonic $W_{18}O_{49}$ nanowires onto carbon fibers by using a facile solvothermal method. We also demonstrated that the carbon fibers obtained by an electrospinning technique could be employed as an excellent low-cost "electron mediator" to greatly boost the separation and transport of IR-excited plasmonic hot electron in $W_{18}O_{49}$ nanowires. Further investigations by ultrafast transient absorption (TA) spectroscopy and finite-difference-time-domain (FDTD) simulations revealed that LSPR excitation of $W_{18}O_{49}$ in the $W_{18}O_{49}$/C heterostructure could lead to the transport of plasmonic hot electron from the $W_{18}O_{49}$ nanowire to the carbon fiber with a very short timescale (~50 fs) and large rate constants ($\sim 2 \times 10^{13}\,s^{-1}$). As such, the $W_{18}O_{49}$/C heterostructure exhibited enhanced catalytic activity for H_2 production from ammonia borane (NH_3BH_3) compared with that of the pure $W_{18}O_{49}$ nanowires upon irradiation by low-energy IR photons.

2. Results and discussion

Fig. 1A shows a schematic illustration of the three-step fabrication route of the $W_{18}O_{49}$/C heterostructure. For the first step, the polyvinylpyrrolidone (PVP) fibers were fabricated by using a traditional electrospinning technique. For the second step, the as-electrospun PVP fibers were carbonized at 900 °C under N_2 atmosphere to prepare the carbon fibers. At last, plasmonic $W_{18}O_{49}$ nanowires were grown onto the above carbon fibers through facile solvothermal method, therefore constructing the $W_{18}O_{49}$/C heterostructure. X-ray diffraction (XRD) patterns of the carbon fibers, $W_{18}O_{49}$/C heterostructures, and $W_{18}O_{49}$ nanowires are given in Fig. 1B. It can be seen that two weak diffraction peaks appear at 25° and 43° for carbon fibers, reflecting to the graphite structure as the (002) plane and the turbostratic carbon structure as (101) plane, respectively. The diffraction peaks on the curve of $W_{18}O_{49}$ nanowires can be indexed to those of monoclinic $W_{18}O_{49}$ (JCPDS No. 05-0392). However, the $W_{18}O_{49}$/C heterostructures showed only the feature peaks of monoclinic $W_{18}O_{49}$. This can be attributed to the low content and poor crystallinity of carbon fibers in $W_{18}O_{49}$/C heterostructures. No impurity peaks were detected from the XRD patterns of $W_{18}O_{49}$/C heterostructures. Scanning electron microscopy (SEM) image in Fig. 1C showed that the electrospun carbon fibers with diameters of 0.6–1.2 μm possess relatively smooth surfaces. After the solvothermal treatment, the entire surfaces of the carbon fibers were decorated with uniform $W_{18}O_{49}$ nanowires, forming the "branch-like" heterostructures (Fig. 1D). Fig. 1E presents the transmission electron microscopy (TEM) image and the corresponding elemental mapping image of an individual $W_{18}O_{49}$/C heterostructure. It is revealed that C element dominant in the middle region of the heterostructure and that W and O elements are mainly distributed at the side.

Further observation by a higher magnification SEM image (Fig. 2A) indicates that the secondary nanostructures of $W_{18}O_{49}$ nanowires on carbon fibers are 10–40 nm in diameters and 0.3–1.2 μm in lengths. Meanwhile, the selected-area electron diffraction (SAED) pattern of the individual $W_{18}O_{49}$/C heterostructure displays two sets of diffraction rings consisting of monoclinic $W_{18}O_{49}$ and graphite carbon (Fig. 2B). These results powerfully confirm the structure of a carbon fiber coated with $W_{18}O_{49}$ nanowires in the $W_{18}O_{49}$/C heterostructure. High-resolution TEM (HRTEM) image (Fig. 2C) illustrates that the $W_{18}O_{49}$

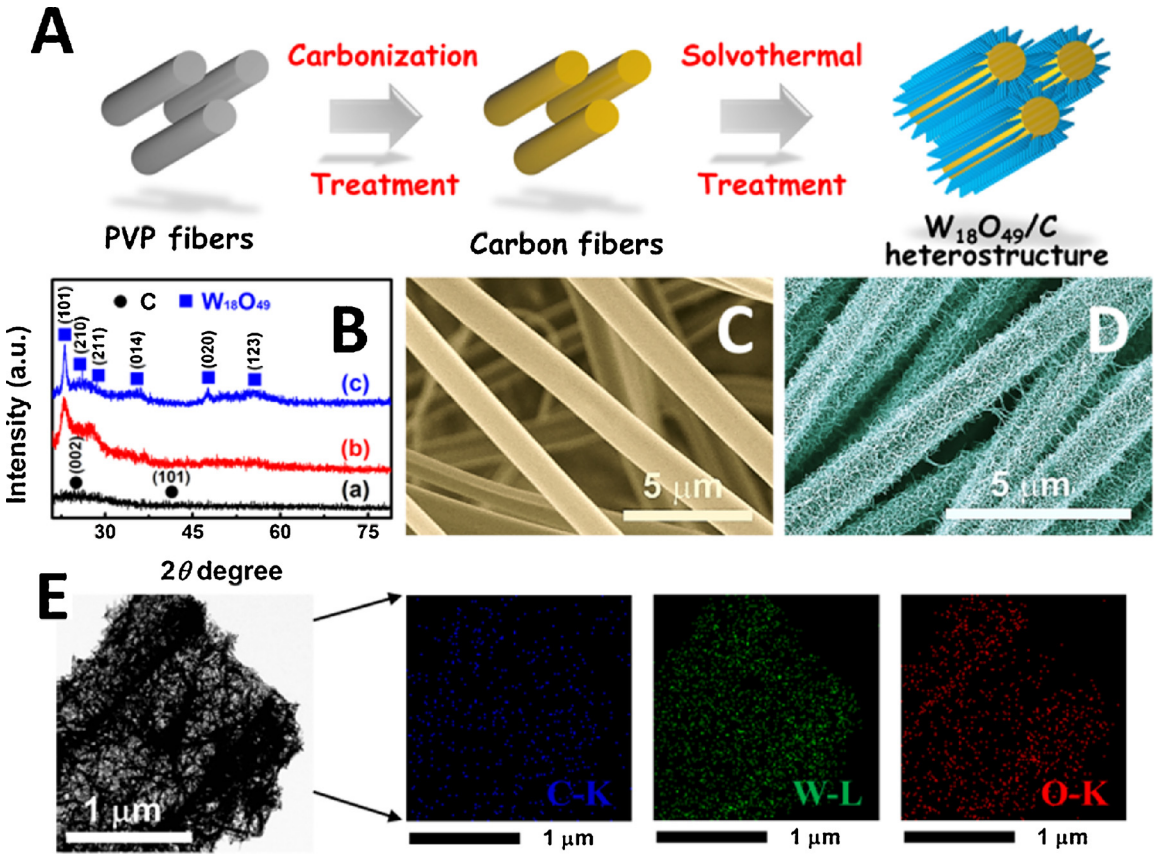

Fig. 1. (A) Schematic diagram of fabrication process of the $W_{18}O_{49}$/C heterostructures; (B) XRD patterns of the as-fabricated (a) carbon fibers; (b) $W_{18}O_{49}$/C heterostructures; (c) $W_{18}O_{49}$ nanowires; SEM images of the (C) carbon fibers and (D) $W_{18}O_{49}$/C heterostructures; (E) TEM and the corresponding elemental mapping images of an individual $W_{18}O_{49}$/C heterostructure.

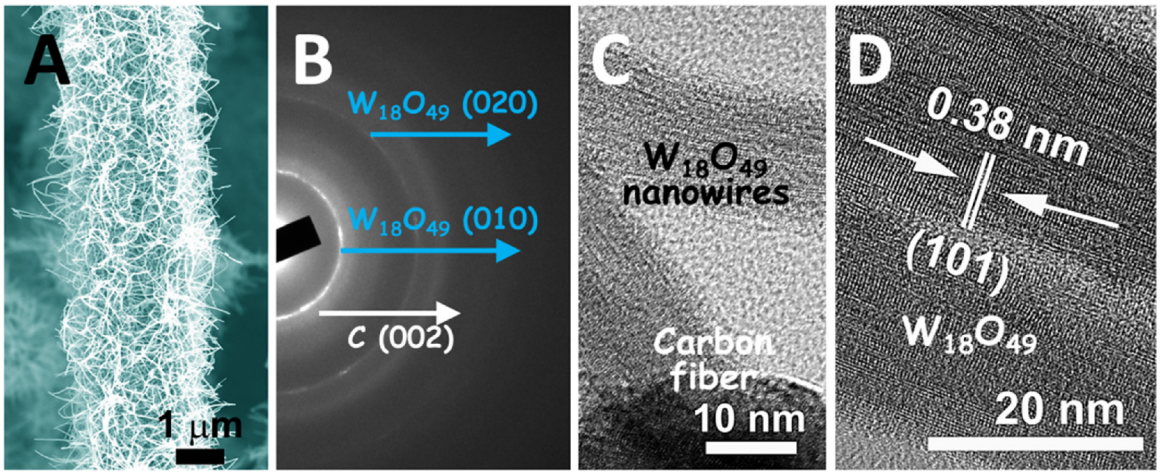

Fig. 2. (A) SEM image of an individual $W_{18}O_{49}$/C heterostructure; (B) SAED pattern of the $W_{18}O_{49}$/C heterostructure; (C, D) HRTEM image of $W_{18}O_{49}$ nanowires on the carbon fiber surface.

nanowire in the heterostructure possesses a bundle structure and is composed of several ultrathin nanowires with diameters from 8 to 15 nm. Furthermore, the lattice-fringe spacing of the above ultrathin nanowire is ~0.38 nm, implying that the $W_{18}O_{49}$ grow along the [010] direction (Fig. 2D).

Fig. 3A shows the Raman spectra of the $W_{18}O_{49}$/C heterostructures in comparison to those of carbon fibers and $W_{18}O_{49}$ nanowires. There are two broad overlapping peaks on the Raman spectrum of the as-electrospun carbon fibers. The peak centered at 1590 cm^{-1} indicates the SP^2 graphite carbon, while 1360 cm^{-1} suggests the defects of SP^3 carbon in carbon fibers [40,41]. The Raman spectrum of $W_{18}O_{49}$ nanowires is dominated by four main vibration peaks at 270, 350, 708, and 805 cm^{-1}, assignable to the bending vibration of δ (O—W—O) and the stretching vibration of ν (W—O—W) of monoclinic phase $W_{18}O_{49}$, respectively [22,42]. The $W_{18}O_{49}$/C heterostructures possess the characteristic Raman peaks of both carbon fibers and $W_{18}O_{49}$ nanowires. The Fourier transform infrared (FT-IR) spectra were carried out to further investigate atomic structures of the as-fabricated samples. In Fig. 3B, there are four peaks on the spectrum of the carbon fibers, which are attributed to the C—C stretching vibration (1200 cm^{-1}), the asymmetric and symmetric stretching band of COO (1540 cm^{-1}), and the —OH stretching modes (1550 and 3420 cm^{-1}), respectively [31,32]. The feature stretching vibration bands, belonging to W = O and O—W—O (500–1000 cm^{-1}), were observed on the spectrum of $W_{18}O_{49}$ nanowires [43,44]. After introducing $W_{18}O_{49}$ nanowires into carbon fibers, the obtained $W_{18}O_{49}$/C heterostructure exhibited the composite FT-IR signals assigned from $W_{18}O_{49}$ nanowires and carbon fibers. Besides, the X-ray photoelectron spectroscopy (XPS) measurements

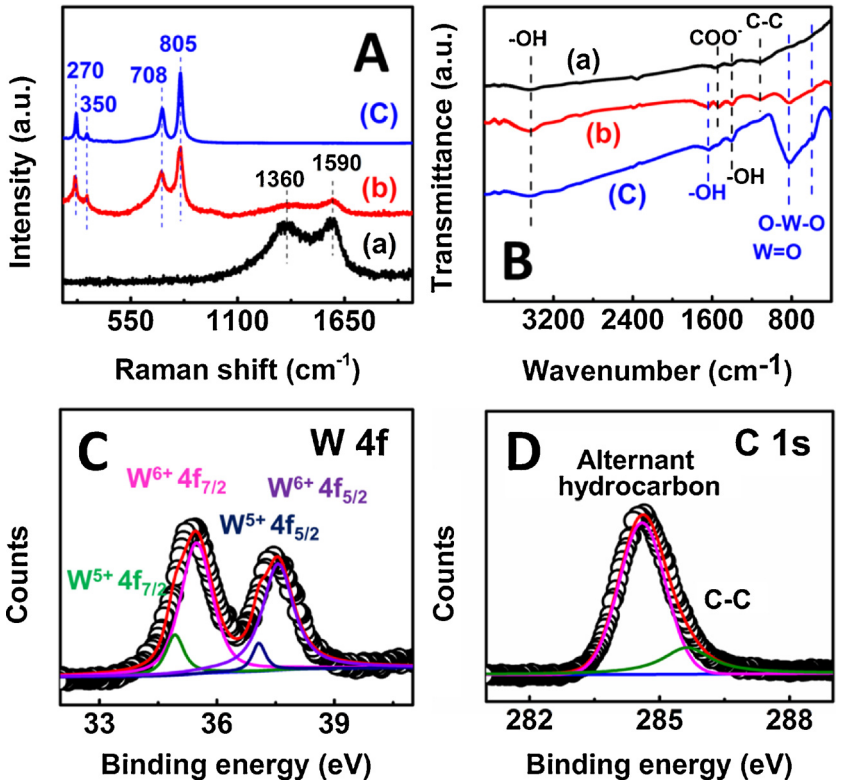

Fig. 3. (A) Raman spectra of (a) carbon fibers; (b) $W_{18}O_{49}$/C heterostructures; (c) $W_{18}O_{49}$ nanowires; (B) FT-IR spectra of (a) carbon fibers; (b) $W_{18}O_{49}$/C heterostructures; (c) $W_{18}O_{49}$ nanowires; XPS spectra of (C) W 4f core-level and (D) C 1 s core-level for the $W_{18}O_{49}$/C heterostructures.

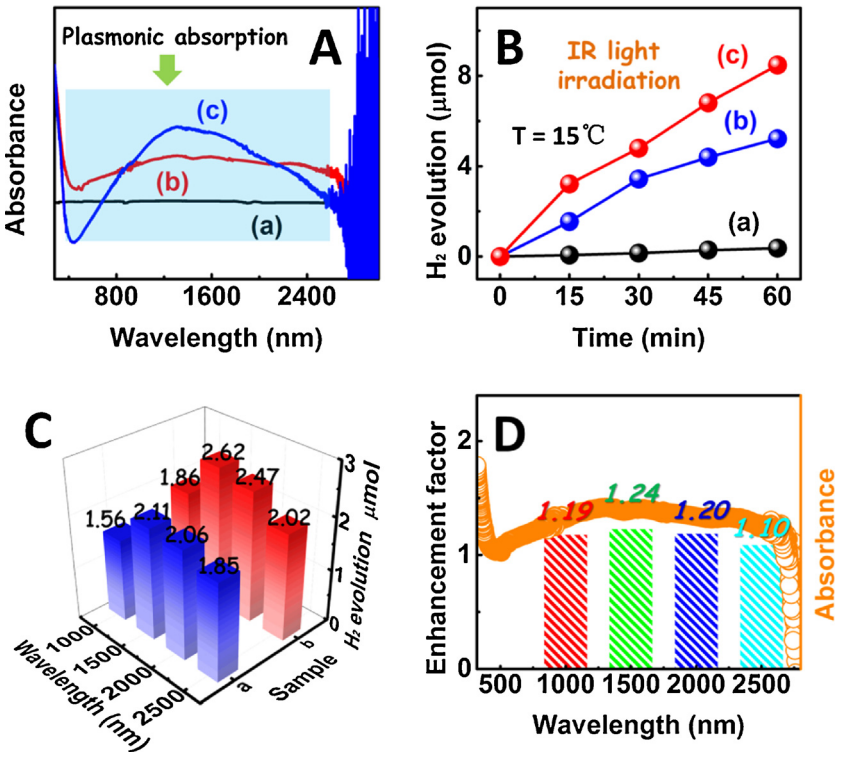

Fig. 4. (A) UV–vis–IR absorption spectra of the as-fabricated (a) carbon fibers; (b) $W_{18}O_{49}$/C heterostructures; (c) $W_{18}O_{49}$ nanowires; (B) time-dependent H_2 production from NH_3BH_3 solution at 15 °C over different samples upon IR-light irradiation: (a) carbon fibers; (b) $W_{18}O_{49}$ nanowires; (c) $W_{18}O_{49}$/C heterostructures; (C) H_2 production amount from NH_3BH_3 solution at 15 °C over (a) $W_{18}O_{49}$ nanowires and (b) $W_{18}O_{49}$/C heterostructures under irradiation at indicated wavelengths for 1 h; (D) wavelength-dependent enhancement factors and plasmonic absorption of $W_{18}O_{49}$/C heterostructures.

revealed that two kinds of W states, including W^{5+} ($4f_{7/2}$: 34.6 eV; $4f_{5/2}$: 37.0 eV) and W^{6+} ($4f_{7/2}$: 35.5 eV; $4f_{5/2}$: 37.6 eV), existed in $W_{18}O_{49}$/C heterostructures (Fig. 3C), which confirmed the formation of the plasmonic component of non-stoichiometric tungsten oxide [19,29]. As observed the C 1 s spectrum in Fig. 3D, the binding energy with peak at 284.6 eV is attributed to the delocalized alternant hydrocarbon, while the peak at 285.6 eV is characteristic of the C—C groups [39]. Based on the above results, it is reasonable to believe that the plasmonic $W_{18}O_{49}$ nanowires have been successfully assembled onto the electrospun carbon fibers to form the 1D "branch-like" heterostructures of $W_{18}O_{49}$/C composite.

The light absorption capacity of the as-fabricated $W_{18}O_{49}$/C heterostructures was studied in comparison to those of $W_{18}O_{49}$ nanowires and carbon fibers through UV–vis–IR absorption spectra. In Fig. 4A, the carbon fibers show a full-spectrum-absorption with a very weak intensity due to the black color of carbon. For the $W_{18}O_{49}$ nanowires, there is a very broad and intense absorption band, ranging from visible to IR region, which can be ascribed to the LSPR, arising from the collective oscillations of excess electrons on the surface of tungsten oxide due to the abundant oxygen vacancies [19,29]. After loading plasmonic $W_{18}O_{49}$ nanowires onto electrospun carbon fibers, the LSPR band could be still observed on the absorption curve of $W_{18}O_{49}$/C heterostructures, even though the absorption intensity was a little lower than that of pure $W_{18}O_{49}$ nanowires.

One potential application of the plasmonic nanostructures is the production of renewable hydrogen energy through catalyzing the hydrogen-carrier molecules [45,46]. Among these molecules, ammonia borane (NH_3BH_3) is the most attractive one, because it stores more than 19.6 wt.% of hydrogen energy, and even exceeds that of gasoline [47,48]. In this work, we employed the catalytic hydrolysis of NH_3BH_3 for H_2 production as the model reaction to evaluate the plasmonic catalytic activity of the $W_{18}O_{49}$/C heterostructures in comparison to that of the single hetero-component. For all catalytic experiments, the reaction temperature was kept at 15 °C by using a connected reflux condenser to weaken the thermally induced catalytic H_2 production. Control experiment in the absence of catalysts showed no H_2 production (Fig. S1). In the dark condition, the pure $W_{18}O_{49}$ nanowires displayed only the H_2 production rate of ~0.02 μmol min^{-1} (Fig. S2), suggesting poor catalytic activity of $W_{18}O_{49}$ without LSPR-excitation. However, upon IR-light irradiation ($\lambda > 750$ nm), the H_2 production rate of $W_{18}O_{49}$ nanowires increased remarkably to ~0.08 μmol min^{-1} (Fig. 4B). This implies that the LSPR-excitation of $W_{18}O_{49}$ nanowires can induce the generation of plasmonic hot electron on their surface for boosting the catalytic H_2 production from NH_3BH_3. In contrast, the electrospun carbon fibers could not drive the release of H_2 from NH_3BH_3 under IR-light irradiation, even though they had a certain light absorption in the IR region. This result reveals that there is no available photo-generated electron on carbon fibers for catalyzing NH_3BH_3 into H_2. Interestingly, when coupling $W_{18}O_{49}$ nanowires with the inert carbon fibers to form $W_{18}O_{49}$/C heterostructures (~0.14 μmol min^{-1}), we observed a 1.75-fold enhancement on the H_2 production as compared to $W_{18}O_{49}$ nanowires. This suggests that in the $W_{18}O_{49}$/C heterostructures, the hetero-component of carbon fibers mainly plays the role of "electron sink" to collect the active plasmonic hot electron from the IR-excited $W_{18}O_{49}$ hetero-component, thereby leading to the improved charge separation and enhanced catalytic activity for H_2 production.

In order to investigate the contribution of hot electron to the H_2 production in this plasmonic heterostructure, we implemented wavelength-dependent catalytic reactions by controlling the incident photon energies at 1000, 1500, 2000, and 2500 nm, respectively. As observed in Fig. 4C, the H_2 production amounts of $W_{18}O_{49}$/C heterostructures are obviously higher than the corresponding values obtained by $W_{18}O_{49}$ nanowires under excitations by the indicated photon energies. Meanwhile, the H_2 production amounts for both two samples are dependent on the excitation wavelengths which are selected according to the LSPR band of $W_{18}O_{49}$ nanowires. Further investigation founded that the enhancement factor, which denoted the ratio value of H_2 production amount between $W_{18}O_{49}$/C heterostructures and $W_{18}O_{49}$ nanowires under the same wavelength excitation, was consistent basically with the absorption band of $W_{18}O_{49}$/C heterostructures in the IR region (Fig. 4D). This observation clearly reveals the enhanced catalytic activity of $W_{18}O_{49}$/C heterostructure is induced by LSPR effect. And, the hetero-component of carbon fibers can act as the "electron mediator" to

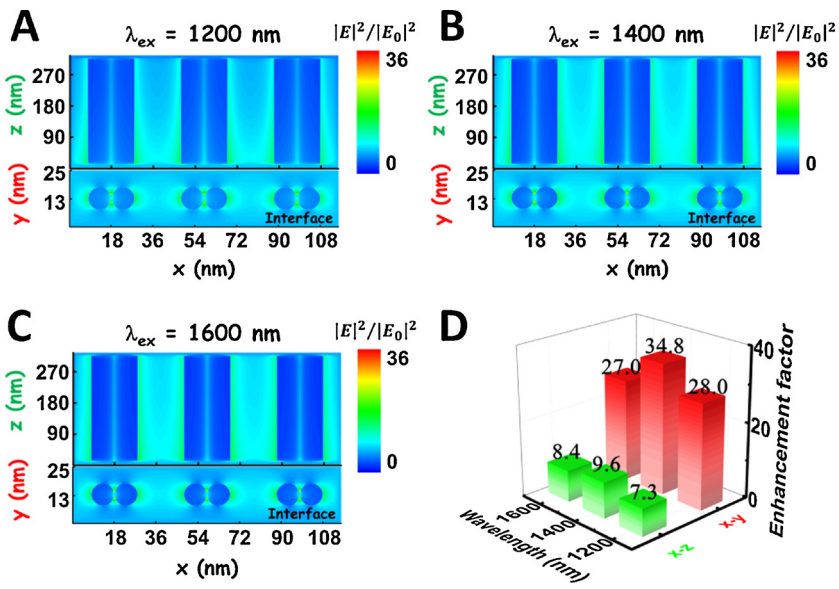

Fig. 5. FDTD simulations of electric field distribution induced by the plasmonic $W_{18}O_{49}$ nanowires and extending into the surrounding carbon fiber for input irradiations at (A) 1200 nm, (B) 1400 nm, and (C) 1600 nm. The incident light was propagated from the y-axis and polarized along the x-axis; (D) wavelength-dependent electric field enhancement at plasmonic hot spots in x–z and z–y planes of the $W_{18}O_{49}$/C heterostructure.

accept the energetic hot electron from the hetero-component of plasmonic $W_{18}O_{49}$ nanowires under IR-light excitation. This IR-driven transfer process of plasmonic hot electron in the $W_{18}O_{49}$/C heterostructure effectively accelerates the catalytic hydrolysis of NH_3BH_3 for releasing H_2.

To understand in-depth the generation of plasmonic hot electron in the $W_{18}O_{49}$/C heterostructure, 3D finite-difference-time-domain (FDTD) simulations were carried out to characterize the LSPR-induced electric field distributions on this heterostructure. A simplified nanostructure of $W_{18}O_{49}$/C was used in the simulation process (Fig. S3), where $W_{18}O_{49}$ component consisted of two ultrathin $W_{18}O_{49}$ nanowires (D = 10 nm; L = 300 nm) supported vertically onto the surface of the carbon fiber (D = 800 nm) with an equal interval of 20 nm. The dielectric function of $W_{18}O_{49}$ was obtained on the basis of first-principles theory. The excitation energies at 1200, 1400, and 1600 nm were used in terms of the plasmonic absorption band of $W_{18}O_{49}$ in the heterostructure (Fig. 4A). As shown in Fig. 5A–C, the LSPR excitation of $W_{18}O_{49}$ hetero-component in the $W_{18}O_{49}$/C heterostructure can significantly enhance the localized electric field to form a plasmonic "hot spot" region near the interface between $W_{18}O_{49}$ nanowires and carbon fiber in both x–y and x–z plane. Moreover, the intensity enhancement ($|E|^2/|E_0|^2$) of localized electric field shows dependence on the excitation wavelength, which matches the LSPR absorption band of the $W_{18}O_{49}$ nanowires. The maximum enhancement factor (~35×) appears under excitation at 1400 nm, which is higher than the corresponding factors obtained at 1200 and 1600 nm excitations (~28× and ~27×, respectively) (Fig. 5D). It is of great significance to note that LSPR-enhanced electric fields are mainly positioned on the surfaces of $W_{18}O_{49}$ nanowires near the surface of carbon fiber, indicating that the plasmonic $W_{18}O_{49}$ can effectively concentrate the incident light field with IR frequencies to generate energetic hot electrons surrounding the $W_{18}O_{49}$/C interface. These plasmon-excited hot electrons on the surfaces of the $W_{18}O_{49}$ nanowires may further transfer to the carbon fiber across the hetero-interface.

To clarify the kinetics process of plasmonic hot electron in the LSPR-excited $W_{18}O_{49}$/C heterostructures, ultrafast transient absorption (TA) spectroscopy measurements were performed on the $W_{18}O_{49}$/C heterostructures and $W_{18}O_{49}$ nanowires for the purpose of comparison. We chose the photon energy at 800 nm (~1.55 eV) to excite the samples, because this energy is below the threshold value for inducing the interband transition of $W_{18}O_{49}$, but can drive the LSPR of $W_{18}O_{49}$. In Fig. 6A, the $W_{18}O_{49}$ nanowires present a broad and intense TA signal with a maximum optical density (OD) at 1045 nm. This absorption signal is formed quickly and disappears in the time scale of tens of picoseconds. This result implies that the LSPR of $W_{18}O_{49}$ nanowires occurs upon 800-nm irradiation, by which the free electrons around the Fermi level (E_f) of the nanowires reach a virtual high-energy surface plasmon (SP) state above the conduction band (CB) of $W_{18}O_{49}$ to form energetic hot electrons [4]. Notably, when loading these plasmonic $W_{18}O_{49}$ nanowires onto carbon fibers to form the heterostructures, the LSPR-induced TA signal appears in a narrow wavelength-range around 1045 nm, and vanishes within hundreds of femtoseconds (Fig. 6B). The above results suggest that, in $W_{18}O_{49}$/C heterostructures, the LSPR-excited hot electrons on the SP state of $W_{18}O_{49}$ hetero-component transfer quickly to the hetero-component of carbon fibers rather than relax to the plasmonic ground state of $W_{18}O_{49}$.

To achieve a better understanding on the above kinetics process, we fixed the probe wavelength at 1045 nm, and used exponential decay functions to fit the corresponding TA curves. As shown in Fig. 6C, the TA decay curves from the $W_{18}O_{49}$ nanowires can be fitted by the following biexponential function:

$$y = A_1 \cdot \exp(-t/\tau_1) + A_2 \cdot \exp(-t/\tau_2) + y_0$$

This result indicates the existence of two decay channels in the $W_{18}O_{49}$ nanowires after LSPR excitation. The time constant (τ_1) of the fast decay process is only ~0.12 ps, which is accordance to the electron-to-phonon scattering time in plasmonic nanostructures. Moreover, the time constant (τ_2) of the slow decay process is ~5.50 ps, which is attributed to the phonon-dielectric medium during the relaxation of hot electrons to the ground state of plasmonic $W_{18}O_{49}$. This kinetics process is reflected to the photothermal effect of plasmonic materials [27,28,39,47–51]. In the case of $W_{18}O_{49}$/C heterostructure, the TA decay curve obeys the monoexponential function fitting:

$$y = A \cdot \exp(-t/\tau) + y_0$$

Only one fast decay process with time constant of ~50 fs can be calculated by using this formula, which reveals the lack of hot-electron relaxation process in the $W_{18}O_{49}$ hetero-component. Furthermore, the average decay time constant (τ_A) of $W_{18}O_{49}$ nanowires can be concluded according to the following formula [49–51]:

$$\tau_A = \frac{A_1 \cdot \tau_1^2 + A_2 \cdot \tau_2^2}{A_1 \cdot \tau_1 + A_2 \cdot \tau_2}$$

The obtained time constant (~4.0 ps) are at least 80 times larger than that of $W_{18}O_{49}$/C heterostructures (50 fs). The disappeared process of slow decay and the decreased average time constant in the $W_{18}O_{49}$/C

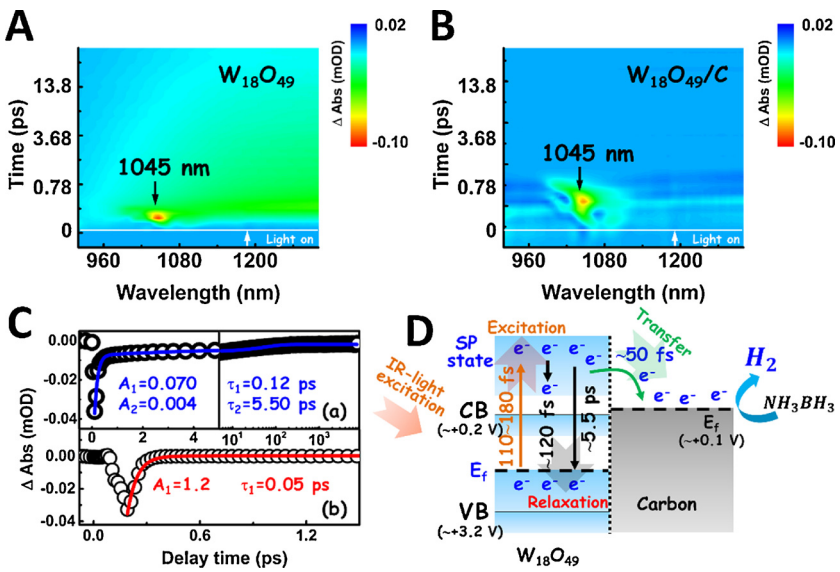

Fig. 6. Ultrafast TA spectra of (A) the $W_{18}O_{49}$ nanowires and (B) the $W_{18}O_{49}$/C heterostructures after 800 nm excitation; (C) TA kinetics curves of (a) the $W_{18}O_{49}$ nanowries and (b) the $W_{18}O_{49}$/C heterostructures with probe wavelength at 1045 nm; (D) schematic of the kinetics process of plasmon-induced hot electrons in the $W_{18}O_{49}$/C heterostructures for enhancing the catalytic H_2 production from NH_3BH_3.

heterostructures powerfully confirm the ultrafast transfer of plasmonic hot electrons from the $W_{18}O_{49}$ nanowires to the carbon fibers. The transfer rate constant (k_{et}) of these plasmonic hot electrons can be estimated as follows [52–54]:

$$k_{et}(W_{18}O_{49}/C \rightarrow W_{18}O_{49}) = \frac{1}{<\tau_A>_{(W_{18}O_{49}/C)}} - \frac{1}{<\tau_A>_{(W_{18}O_{49})}}$$

It can be found that, upon LSPR excitation at 800 nm, the transfer rate constant is $\sim 2 \times 10^{13}\,s^{-1}$. Notably, this transfer rate constant is 10^3–10^5 times larger than the values obtained in traditional semiconductor heterostructure systems [52–54], which further demonstrates that the ultrafast electron transfer process in non-metallic $W_{18}O_{49}$/C heterostructures is driven by the LSPR excitation of the $W_{18}O_{49}$ hetero-component. Furthermore, it is also proven that the electrospun carbon fibers is an excellent "electron mediator" to hinder the recombination of plasmonic hot electrons.

Based on the above experimental results and simulation analyses, the kinetics process of plasmon-induced hot-electron transfer on the enhanced catalytic H_2 production over the plasmonic $W_{18}O_{49}$/C heterostructure was proposed, as shown in Fig. 6D. Upon IR irradiation to excite the LSPR of the $W_{18}O_{49}$ hetero-component in $W_{18}O_{49}$/C heterostructures, the excess free electrons around the E_f of the $W_{18}O_{49}$ can reach a high-energy SP state to generate the plasmonic hot electrons (110–180 fs), which then transfer to the adjacent carbon fiber surface with very large rate constant of $\sim 2 \times 10^{13}\,s^{-1}$. Importantly, the time scale associated with the transfer of the hot electrons from the $W_{18}O_{49}$ to the carbon fiber (~50 fs) is shorter than the time scales associated with the relaxation of hot electrons on the SP state (~120 fs) or back to the E_f of the $W_{18}O_{49}$ (5.5 ps). As such, when the $W_{18}O_{49}$/C heterostructures is excited by low-energy IR light, a plenty of plasmon-excited hot electrons would transfer from the $W_{18}O_{49}$ to the carbon fibers' surface, fulfilling the catalytic hydrolysis of NH_3BH_3 for H_2 production.

3. Conclusions

In summary, we successfully fabricated 1D $W_{18}O_{49}$/C heterostructures through solvothermal growth of $W_{18}O_{49}$ nanowires onto electrospun carbon fibers. By using ultrafast TA spectroscopy and FDTD simulations, we proved that electrospun carbon fibers could be served as an excellent low-cost "electron mediator" to boost the transfer and separation of IR-excited hot electron in plasmonic $W_{18}O_{49}$ nanowires. Further investigations founded that the transfer of IR-excited plasmonic hot electrons from the $W_{18}O_{49}$ to the carbon fibers was completed within only ~50 fs in the heterostructures, which is much faster than their relaxation process from the high-energy SP to the ground state (5.5 ps) in the $W_{18}O_{49}$ nanowires. In this way, the generation and separation of plasmonic hot electrons in $W_{18}O_{49}$/C heterostructures were remarkably promoted, thereby resulting in an enhanced catalytic activity for H_2 production from NH_3BH_3 compared with the activity of pure $W_{18}O_{49}$ nanowires. This work provides a new insight on the design and construction of a highly-efficient IR-driven photocatalyst through combining the plasmonic semiconductor nanostructure and a low-cost non-metallic "electron mediator".

Acknowledgements

This work is supported by the National Natural Science Foundation of China (Grant Nos: 51772041, 11474046, 61775024, and 21503034), Natural Science Foundation of Liaoning Province (20170540190), the Program for Liaoning Excellent Talents in University (LNET) (Grant No. LR2015016), the Program for Dalian Excellent Talents (Grant No. 2016RQ069), and the Science and Technique Foundation of Dalian (Grant Nos. 2014J11JH134 and 2015J12JH201).

Appendix A. Supplementary data

Supplementary material related to this article can be found, in the online version, at doi:https://doi.org/10.1016/j.apcatb.2018.03.073.

References

[1] X. Zou, Y. Zhang, Chem. Soc. Rev. 44 (2015) 5148–5180.
[2] K. Shimura, H. Yoshida, Energy Environ. Sci. 4 (2011) 2467–2481.
[3] H. Kisch, Angew. Chem. Int. Ed. 52 (2013) 812–847.
[4] Z. Zhang, X. Jiang, B. Liu, L. Guo, N. Lu, L. Wang, J. Huang, K. Liu, B. Dong, Adv. Mater. (2018).
[5] P.Y. Kuang, P.X. Zheng, Z.Q. Liu, J.L. Lei, H. Wu, N. Li, T.Y. Ma, Small 12 (2016) 6735–6744.
[6] G. Cui, W. Wang, M. Ma, J. Xie, X. Shi, N. Deng, J. Xin, B. Tang, Nano Lett. 15 (2015) 7199.
[7] R. Marschall, Adv. Funct. Mater. 24 (2014) 2421–2440.
[8] Y. Sang, Z. Zhao, M. Zhao, P. Hao, Y. Leng, H. Liu, Adv. Mater. 27 (2015) 363–369.
[9] Y.P. Yuan, L.W. Ruan, J. Barber, S.C.J. Loo, C. Xue, Energy Environ. Sci. 7 (2014) 3934–3951.
[10] Z. Gan, Z. Chen, L. Liu, L. Zhang, W. Tu, Y. Liu, Sol. RRL 1 (2017) 1600032.
[11] Z. Zhang, Y. Huang, K. Liu, L. Guo, Q. Yuan, B. Dong, Adv. Mater. 27 (2015) 5906.
[12] M. Bilokur, A. Gentle, M.D. Arnold, M.B. Cortie, G.B. Smith, Sol. RRL 1 (2017) 1700092.
[13] S. Linic, P. Christopher, D.B. Ingram, Nat. Mater. 10 (2011) 911.
[14] Z. Lou, M. Fujitsuka, T. Majima, ACS Nano 10 (2016) 6299.
[15] R.B. Wei, P.Y. Kuang, H. Cheng, Y.B. Chen, J.Y. Long, M.Y. Zhang, Z.Q. Liu, ACS Sustain. Chem. Eng. 5 (2017) 4249–4257.
[16] T.T. Zhuang, Y. Liu, Y. Li, Y. Zhao, L. Wu, J. Jiang, S.H. Yu, Angew. Chem. Int. Ed.

55 (2016) 6396.
[17] J. Cui, Y. Li, L. Liu, L. Chen, J. Xu, J. Ma, G. Fang, E. Zhu, H. Wu, L. Zhao, Nano Lett. 15 (2015) 6295.
[18] Z. Zhu, P. Huo, Z. Lu, Y. Yan, Z. Liu, W. Shi, C. Li, H. Dong, Chem. Eng. J. 331 (2018) 615–625.
[19] Z. Zhang, J. Huang, Y. Fang, M. Zhang, K. Liu, B. Dong, Adv. Mater. 29 (2017) 1606688.
[20] R.B. Wei, Z.L. Huang, G.H. Gu, Z. Wang, L. Zeng, Y. Chen, Z.Q. Liu, Appl. Catal. B Environ. 231 (2018) 101–107.
[21] Z. Zhu, Z. Lu, D. Wang, X. Tang, Y. Yan, W. Shi, Y. Wang, N. Gao, X. Yao, H. Dong, Appl. Catal. B Environ. 182 (2016) 115–122.
[22] J. Yan, T. Wang, G. Wu, W. Dai, N. Guan, L. Li, J. Gong, Adv. Mater. 27 (2015) 1580–1586.
[23] Q. Xu, B. Zhu, C. Jiang, B. Cheng, J. Yu, Sol. RRL 2 (2018) 1800006.
[24] Z. Zhu, Y. Yu, H. Dong, Z. Liu, C. Li, P. Huo, Y. Yan, ACS Sustain. Chem. Eng. 5 (2017) 10614–10623.
[25] D. Mocatta, G. Cohen, J. Schattner, O. Millo, E. Rabani, U. Banin, Science 332 (2011) 77.
[26] D. Zhou, D. Liu, W. Xu, Z. Yin, X. Chen, P. Zhou, S. Cui, Z. Chen, H. Song, ACS Nano 10 (2016) 5169.
[27] H. Cheng, T. Kamegawa, K. Mori, H. Yamashita, Angew. Chem. Int. Ed. 53 (2014) 2910–2914.
[28] G. Xi, S. Ouyang, P. Li, J. Ye, Q. Ma, N. Su, H. Bai, C. Wang, Angew. Chem. Int. Ed. 51 (2012) 2395.
[29] Z. Lou, Q. Gu, L. Xu, Y. Liao, C. Xue, Chem. Asian J. 10 (2015) 1291–1294.
[30] Z. Lou, G. Quan, Y. Liao, S. Yu, C. Xue, Appl. Catal. B Environ. 184 (2016) 258–263.
[31] Y. Chen, G. Tian, Z. Ren, K. Pan, Y. Shi, J. Wang, H. Fu, ACS Appl. Mater. Interfaces 6 (2014) 13841.
[32] J. Mu, C. Shao, Z. Guo, Z. Zhang, M. Zhang, P. Zhang, B. Chen, Y. Liu, ACS Appl. Mater. Interfaces 3 (2011) 590.
[33] L. Zhang, D. Austin, V.I. Merkulov, A.V. Meleshko, Appl. Phys. Lett. 84 (2004) 3972–3974.
[34] J. Mu, B. Chen, Z. Guo, M. Zhang, Z. Zhang, C. Shao, Y. Liu, J. Colloid Interface Sci. 356 (2011) 706–712.
[35] P. Zhang, C. Shao, X. Li, M. Zhang, X. Zhang, C. Su, N. Lu, K. Wang, Y. Liu, Phys. Chem. Chem. Phys. 15 (2013) 10453.
[36] L. Li, X. Zhang, Z. Zhang, M. Zhang, L. Cong, Y. Pan, S. Lin, J. Mater. Chem. A 4 (2016) 16635–16644.
[37] T. Zhu, H.B. Wu, Y. Wang, R. Xu, X.W. Lou, Adv. Energy Mater. 2 (2012) 1497–1502.
[38] J. Mu, C. Shao, Z. Guo, M. Zhang, Z. Zhang, P. Zhang, B. Chen, Y. Liu, J. Mater. Chem. 22 (2012) 1786–1793.
[39] P. Zhang, C. Shao, Z. Zhang, M. Zhang, J. Mu, Z. Guo, Y. Liu, Nanoscale 3 (2011) 3357.
[40] Z. Zhang, X. Li, C. Wang, S. Fu, Y. Liu, C. Shao, Macromol. Mater. Eng. 294 (2009) 673–678.
[41] M. Inagaki, Y. Yang, F. Kang, Adv. Mater. 24 (2012) 2547.
[42] A. Wolcott, T.R. Kuykendall, W. Chen, S. Chen, J.Z. Zhang, J. Phys. Chem. B 110 (2006) 25288.
[43] J. Polleux, N. Pinna, M. Antonietti, M. Niederberger, J. Am. Chem. Soc. 127 (2005) 15595–15601.
[44] J. Liu, O. Margeat, W. Dachraoui, X. Liu, M. Fahlman, J. Ackermann, Adv. Funct. Mater. 24 (2014) 6029–6037.
[45] K. Fuku, R. Hayashi, S. Takakura, T. Kamegawa, K. Mori, H. Yamashita, Angew. Chem. Int. Ed. 52 (2013) 7446–7450.
[46] H. Cheng, X. Qian, Y. Kuwahara, K. Mori, H. Yamashita, Adv. Mater. 27 (2015) 4616.
[47] M. Yadav, Q. Xu, Energy Environ. Sci. 5 (2012) 9698–9725.
[48] J.M. Yan, X.B. Zhang, T. Akita, M. Haruta, Q. Xu, J. Am. Chem. Soc. 132 (2010) 5326.
[49] Y.C. Chen, Y.C. Pu, Y.J. Hsu, J. Phys. Chem. C 116 (2012) 2967–2975.
[50] T.T. Yang, W.T. Chen, Y.J. Hsu, K.H. Wei, T.Y. Lin, T.W. Lin, J. Phys. Chem. C 114 (2010) 11414–11420.
[51] X. Wang, C. Liow, A. Bisht, X. Liu, T.C. Sum, X. Chen, S. Li, Adv. Mater. 27 (2015) 2207–2214.
[52] K. Das, S.K. De, J. Phys. Chem. C 113 (2009) 3494–3501.
[53] Z.F. Bian, T. Tachikawa, W. Kim, W. Choi, T. Majima, J. Phys. Chem. C 116 (2012) 25444–25453.
[54] Z. Zhang, K. Liu, Y. Bao, B. Dong, Appl. Catal. B Environ. 203 (2017) 599–606.